

We are IntechOpen, the world's leading publisher of Open Access books Built by scientists, for scientists

4,800

Open access books available

122,000

International authors and editors

135M

Downloads

Our authors are among the

154

Countries delivered to

TOP 1%

most cited scientists

12.2%

Contributors from top 500 universities



WEB OF SCIENCE™

Selection of our books indexed in the Book Citation Index
in Web of Science™ Core Collection (BKCI)

Interested in publishing with us?
Contact book.department@intechopen.com

Numbers displayed above are based on latest data collected.

For more information visit www.intechopen.com



Nanofibrous Scaffolds of Bio-polyesters: In Vitro and In Vivo Characterizations and Tissue Response

Hui Ying Tang^{1,2}, Daisuke Ishii³, Kumar Sudesh¹,
Tetsuji Yamaoka⁴ and Tadahisa Iwata^{2,5}

¹*School of Biological Sciences, Universiti Sains Malaysia, 11800 Penang,*

²*Bioengineering Laboratory, RIKEN Institute /Hirosawa 2-1, Wako-shi, Saitama 351-0198,*

³*Department of Materials Chemistry, Faculty of Science and Engineering, Ryukoku
University / 1-5 Yokotani, Seta Oe-cho, Otsu-shi, Shiga 520-2194,*

⁴*Department of Biomedical Engineering, Advanced Medical Engineering Center, National
Cardiovascular Center Research Institute, 5-7-1 Fujishirodai, Suita-shi, Osaka 565-8565,*

⁵*Department of Biomaterial Sciences, Graduate School of Agricultural and Life Sciences,
The University of Tokyo / 1-1-1 Yayoi, Bunkyo-ku, Tokyo 113-8657,*

¹*Malaysia*

^{2,3,4,5}*Japan*

1. Introduction

1.1 Nanofibers as tissue-engineering scaffolds

Tissue engineering can be broadly defined as the process of creating living, physiological, three-dimensional tissues and organs utilizing specific combination of cells, cell scaffolds, and cell signals, both chemical and mechanical (Griffith, 2000). It offers a promising alternative to donor tissues which are often in short supply. In tissue-engineering, biomaterials are fashioned into scaffolds that can replace the natural extracellular matrix (ECM) until host cells can repopulate and re-synthesize a new natural matrix.

For tissue engineering, apart from the supercellular and cellular scale structures, the subcellular and nanoscale structures are also essential for the control of cellular environment, cell-molecular interactions and cell-cell interactions. It is not surprising that more tissue engineering studies are gearing towards miniaturization at these scales in efforts to mimic the fibrillar structure of the ECM. One such effort is the use of electrospinning, a simple yet versatile method, to produce nanofibers with morphological similarities to the ECM. Nanofibers generally refer to fibers with diameter less than 1 micron. Nanofibers are attractive for tissue engineering in several ways. First, very high surface area-to-volume ratio and high porosity can be achieved for better cell adhesion and growth. Second, the nanofibers possess enhanced mechanical properties compared to the solid-walled equivalents. Third, the ECM-mimicking structures may improve cellular response and biocompatibility.

Polyhydroxyalkanoates (PHAs), a class of naturally derived polyesters, are popular biomaterials for biomedical applications because they are bioabsorbable and biocompatible.

Source: Nanofibers, Book edited by: Ashok Kumar,
ISBN 978-953-7619-86-2, pp. 438, February 2010, INTECH, Croatia, downloaded from SCIYO.COM

They are produced by various bacteria as intracellular carbon and energy compound under unfavorable growth conditions such as limitation of nitrogen, phosphorus, oxygen or magnesium in the presence of excess supply of carbon source (Anderson & Dawes, 1990). Of the PHAs, the poly(4-hydroxybutyrate) [P(4HB)] is rapidly gaining recognition as a new absorbable material for implantable medical applications because it offers new set of properties that are not currently available (Martin & Williams, 2003). A recent major breakthrough for P(4HB) is the clearance obtained from the Food and Drug Administration of the United States of America for the use of P(4HB)-derived TephafLEX® absorbable suture (<http://www.fda.gov/bbs/topics/NEWS/2007/NEW01560.html>). Hence, this book chapter focuses on the potential of the copolymer of P(4HB), that is the poly[(*R*)-3-hydroxybutyrate-co-97mol%-4-hydroxybutyrate] [P(3HB-co-97mol%-4HB)] as a biomaterial for electrospun nanofibrous scaffold. Its performance as a tissue-engineering scaffold was compared with scaffolds derived from poly[(*R*)-3-hydroxybutyrate] [P(3HB)] and its copolymers; poly[(*R*)-3-hydroxybutyrate-co-5mol%-(*R*)-3-hydroxyhexanoate] [P(3HB-co-5mol%-3HHx)] and poly[(*R*)-3-hydroxybutyrate-co-7mol%-4-hydroxybutyrate] [P(3HB-co-7mol%-4HB)]. Since bio-polyesters based on lactide monomers are the workhorse synthetic polymers for scaffold fabrication, the performance aspects of nanofibrous scaffolds made from PHAs were compared with those derived from synthetic polyesters; poly(L-lactide) (PLLA) and stereocomplexed PLA. The chemical structures of these biopolyesters are shown in Figure 1. Subcutaneous implantation of the nanofibrous scaffolds in rats was performed to investigate their bioabsorption behavior and tissue response. The nanofibrous scaffolds before and after the *in vitro* and *in vivo* experiments were characterized using scanning electron microscopy (SEM), X-ray diffraction, gel permeation chromatography and tensile test. Tissue response was also determined by histological evaluation. Our findings reported here had been published in our earlier works (Ishii et al., 2007; Tang et al., 2009; Ishii et al., 2009).

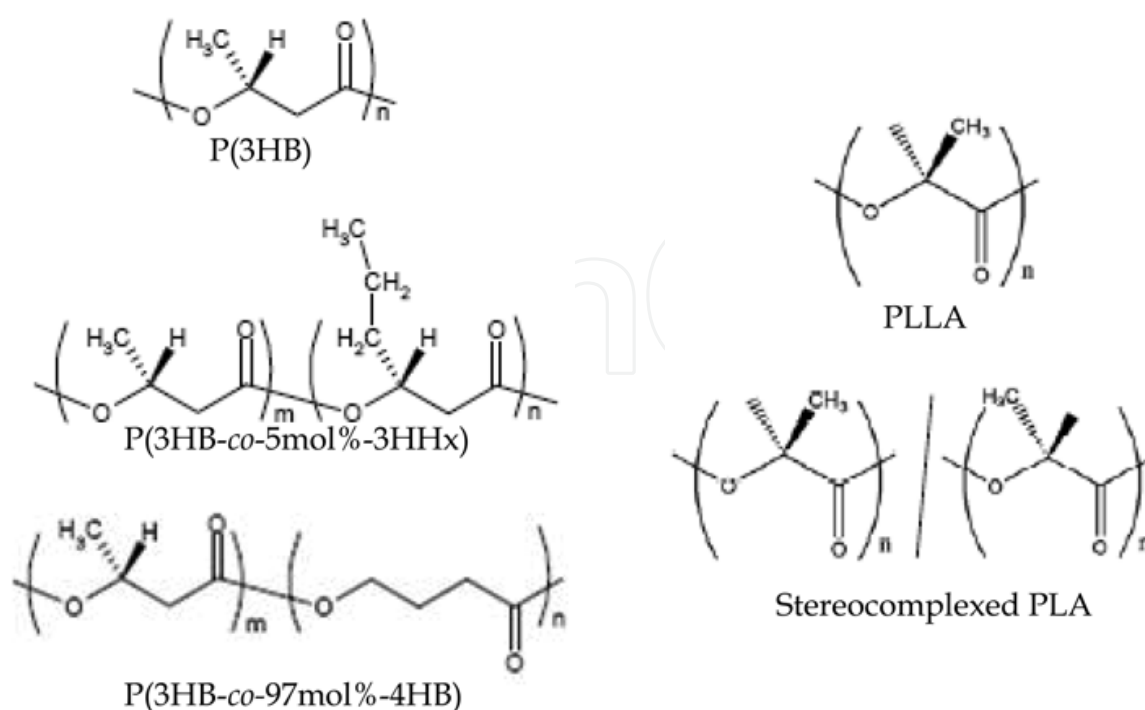


Fig. 1. Chemical structures of PHAs, PLLA and stereocomplexed PLA.

2. Preparation of PHA and PLA-based nanofibrous scaffolds by electrospinning

The electrospinning apparatus is quite simple, consisting only three major components: a high voltage power supply, a polymer solution reservoir (usually a syringe with a small diameter needle) with or without a flow control pump and a metal collecting plate. To initiate the electrospinning process, the polymers are dissolved in the appropriate solvent and loaded into the polymer reservoir. Once a source electrode is attached to the syringe, an electric field between the polymer solution and a grounded target is created by a high-voltage power source. The electrostatic field at the syringe-air interface competes with the surface tension of the liquid solution. A semispherical polymer solution droplet is formed at the tip of the needle when the polymer solution is extruded slowly by a syringe pump and/or gravity. With increasing voltage, the polymer droplet elongates to form a conical shape known as the Taylor cone (Subbiah et al., 2005). When the critical voltage is reached, the surface tension is overcome by the electrostatic force and a polymer jet is initiated (Taylor, 1964). The surface charge on the jet is further increased as the solvent in the polymer jet evaporates when drawn to the collecting plate. This increase in surface charge induces instability in the polymer jet as it passes through the electric field (Demir et al., 2004). Hence, the polymer jet divides geometrically, first into two jets, and then into many more as the process repeats itself to compensate for the instability. The formation of fibers results from the action of the spinning force provided by the electrostatic force on the continuously splitting polymer droplets. A non-woven nanofibrous scaffold is eventually formed when the nanofibers are deposited layer-by-layer on the metal collecting plate.

3. *In Vitro* and *In Vivo* characterizations of PHA and PLA-based nanofibrous scaffolds

3.1 Morphology of nanofibrous scaffolds

As revealed by SEM, all electrospun nanofibrous scaffolds spun from 1,1,1,3,3,3-hexafluoro-2-propanol (HFIP) consist of randomly oriented nanofibers (Figs. 2, 3 and 4). The width of the nanofibers between the junctions was quite uniform. The width decreased in the order of P(3HB) \approx P(3HB-co-5mol%-3HHx) (520 nm) > PLLA \approx stereocomplexed PLA (300 nm) > P(3HB-co-97mol%-4HB) (220 nm) > P(3HB-co-7mol%-4HB) (190 nm). The increment in width is proportional to the molecular weight of the polymer (Dong, 2004) because higher degree of chain entanglement due to high molecular weight is assumed to make it harder for the electrostatic forces to pull, or extend individual chains (Lyons et al., 2004). As such, the matrices of the electrospun P(3HB) and P(3HB-co-5mol%-3HHx) consisted of larger nanofibers compared to the electrospun P(3HB-co-97mol%-4HB) and PLA-based nanofibrous scaffolds because of their high molecular weight (Table 1). Interestingly, only the electrospun P(3HB-co-7mol%-4HB) formed nanofibers with irregular shapes with intermittent spindle-like beads on string (Fig. 3A). Possibly the formation of the beaded P(3HB-co-7mol%-4HB) nanofibers is the result of low net charge density as shown by previous studies (Fong et al. 1999; Zuo et al., 2005). According to Dong et al., the net charge density is inversely proportional to the mass of dry polymer (i.e. mass of scaffolds collected from electrospinning), if the other experimental conditions such as jet current, collecting time and polymer concentration are the same. The net charge density decreases in the order of P(3HB-co-5mol%-3HHx) (1058 Coulomb/liter) > P(3HB) (1002 Coulomb/liter) > P(3HB-co-97mol%-4HB) (778 Coulomb/liter) > P(3HB-co-7mol%-4HB) (484 Coulomb/liter).

After sterilization, the morphologies observed for the electrospun P(3HB), P(3HB-co-5mol%-3HHx), P(3HB-co-7mol%-4HB) and PLA-based nanofibrous scaffolds remained unchanged (Figs. 2, 3 and 4). The matrix of P(3HB-co-97mol%-4HB), however, became less porous (Fig. 3 B2). The temperature (40 °C) of the ethylene oxide (EtO) sterilization is close to the melting temperature of P(3HB-co-97mol%-4HB) ($T_m = 47$ °C), and thus led to the fusing of some nanofibers to each other.

3.1 (a) *In Vitro* study

After 4 weeks of immersion in phosphate buffered saline (PBS), there was no evidence of degradation on the surface of all the electrospun PHA scaffolds. The structural integrities of the PHA nanofibrous scaffolds were maintained even after 12 weeks. This is because PHA hardly undergoes hydrolysis at pH value around neutrality. Interestingly, the electrospun P(3HB-co-97mol%-4HB) and PLA-based nanofibrous scaffolds appeared to have swollen. Possibly, the swelling of these nanofibers was caused by the penetration of water into their amorphous regions as reported in the literature concerning electrospun Poly(D,L-lactic-co-glycolic acid), poly(D,L-lactic acid) and poly(butylene succinate) fibers after immersion in PBS (Zong et al., 2003; Jeong et al., 2005; Li et al., 2006). The PLLA nanofibers showed the most pronounced swelling (width of nanofibers increased from 300 nm to 1200 nm) compared to the stereocomplexed PLA nanofibers (width of nanofibers increased from 300 nm to 600 nm). It is believed that the strong interaction between the molecular chains of PLLA and PDLA in the stereocomplexed PLA fibers might limit their swelling in PBS. In accordance to this observation, only the PLLA fibers showed fragmentation after 4 weeks in PBS. However, after 12 weeks in PBS, both the PLLA and stereocomplexed PLA fibers showed cleavage.

3.1 (b) *In Vivo* study

In SEM, only the remaining scaffolds that could be retrieved from rat after the *in vivo* experiments were observed. Nevertheless, such observations provided the information on the morphological changes by implantation. No remarkable change was observed for the P(3HB) and P(3HB-co-5mol%-3HHx) nanofibrous scaffolds during the period of implantation (Fig. 2). In contrast, the nanofibers of the copolymers with 4HB unit were affected by the implantation. At 4 weeks of implantation, the nanofibers of P(3HB-co-97mol%-4HB) showed fragmentation (Fig. 3 B3). After 12 weeks, surface erosion became more evident as the density of the nanofibers decreased remarkably due to fragmentation of the fibers to shorter segments. The progression of bioabsorption was also evidenced by the formation of pores on the surface of these fibers as indicated by the arrow in Fig. 3 B4. These evidences indicate that the existence of 4HB monomer units enhances the degradability, or the bioabsorption of PHA. As for the PLLA nanofibrous scaffold, cleavage of the nanofiber strands occurred after 4 weeks of implantation (Fig. 4 A3). A decrease in the density of the nanofibers in the scaffold was observed after 12 weeks. The stereocomplexed PLA nanofibrous scaffold remained in its original state even after 12 weeks of implantation (Fig. 4 B4).

The *in vitro* and *in vivo* observations using SEM revealed significant difference in the bioabsorption behavior of the electrospun PHA and PLA-based scaffolds. For the electrospun PHA scaffolds, fibers with smaller diameter were more prone to fragmentation because of increased water contact due to large surface area. However, for the electrospun

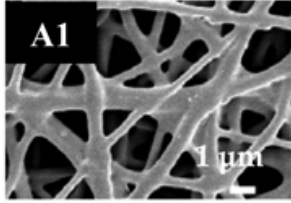
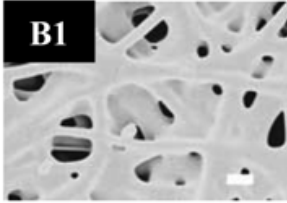
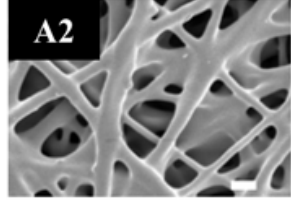
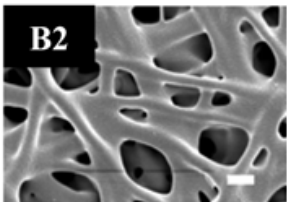
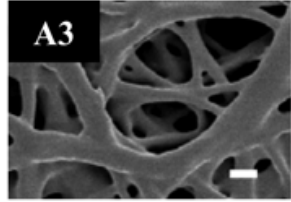
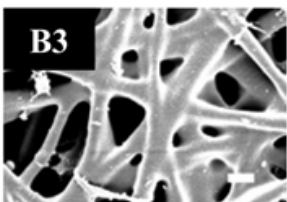
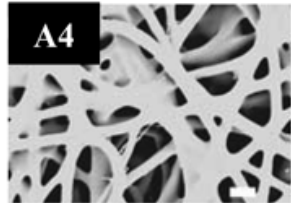

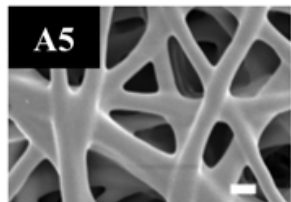
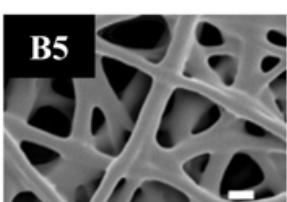
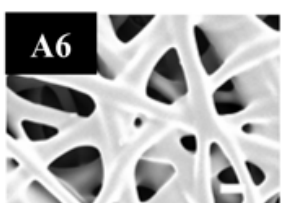
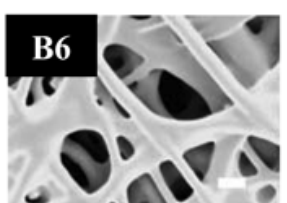
| Condition | Material | |
|--------------------------|---|---|
| | P(3HB) | P(3HB-co-5mol%-3HHx) |
| As-spun |  |  |
| Sterilized |  |  |
| 4 weeks <i>in vivo</i> |  |  |
| 12 weeks <i>in vivo</i> |  |  |
| 4 weeks <i>in vitro</i> |  |  |
| 12 weeks <i>in vitro</i> |  |  |

Fig. 2. SEM micrographs of the electrospun P(3HB) and P(3HB-co-5mol%-3HHx) in various conditions.

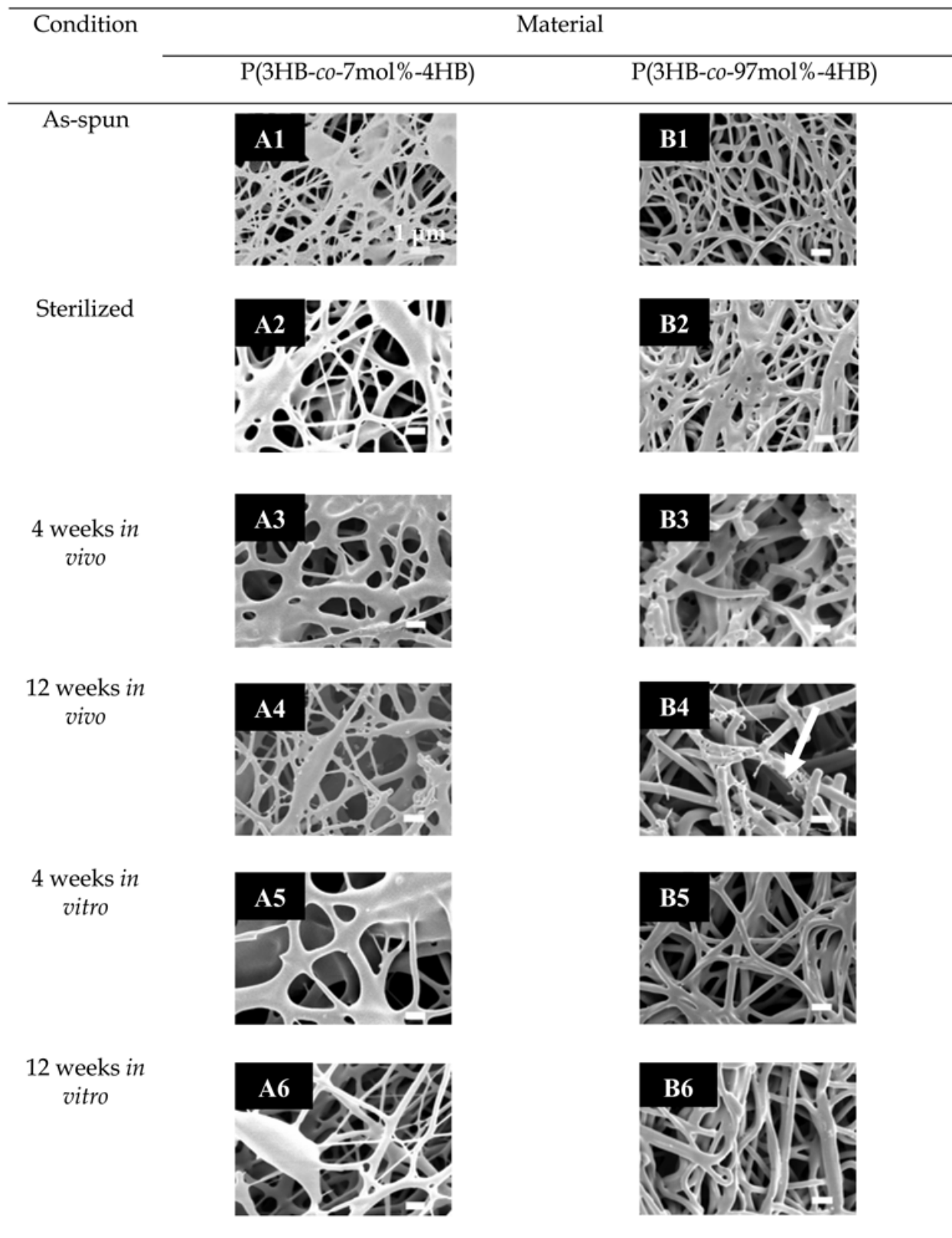


Fig. 3. SEM micrographs of the electrospun P(3HB-co-7mol%-4HB) and P(3HB-co-97mol%-4HB) in various conditions. The arrow shows the pores on the nanofiber.

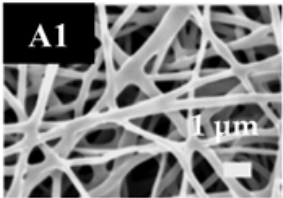
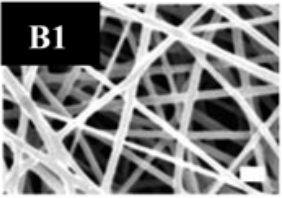
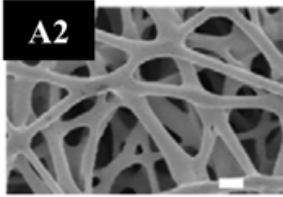
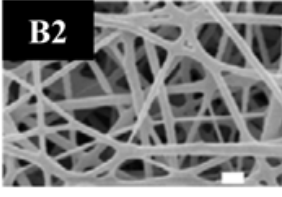
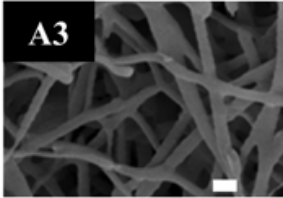
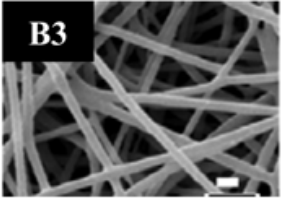
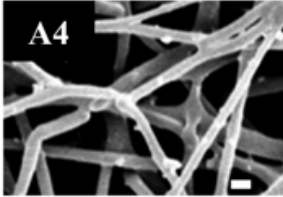
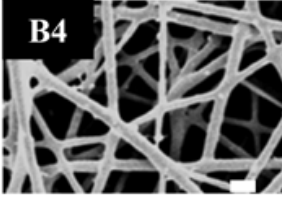

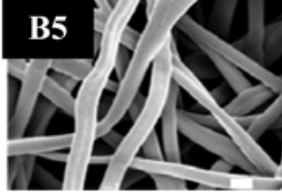
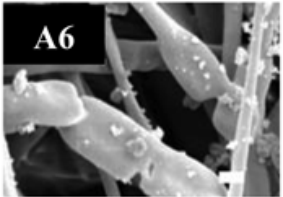
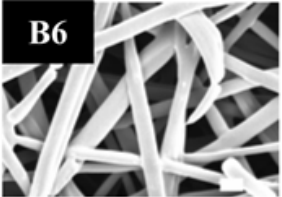
| Condition | Material | |
|--------------------------|---|---|
| | PLLA | Stereocomplexed PLA |
| As-spun |  |  |
| Sterilized |  |  |
| 4 weeks <i>in vivo</i> |  |  |
| 12 weeks <i>in vivo</i> |  |  |
| 4 weeks <i>in vitro</i> |  |  |
| 12 weeks <i>in vitro</i> |  |  |

Fig. 4. SEM micrographs of the electrospun PLLA and stereocomplexed PLA in various conditions.

PLA-based scaffolds consisting of the same average fiber diameter, the water uptake ability of the fibers becomes the determining factor of their bioabsorption rate. Unlike the electrospun PHA scaffolds, the exposure to PBS brings more detrimental effects to the fiber structure of the PLA-based scaffolds which are known to be susceptible to hydrolysis. Thus, it can be concluded that while the surface erosion of the electrospun PHA scaffolds is dependent on the individual fiber dimensions and monomeric content, the bioabsorption of the electrospun PLA-based scaffolds is dependent on the water uptake ability.

3.2 Crystallinity of nanofibrous scaffolds

The WAXD profiles of the as-spun PHA nanofibrous scaffolds are displayed in Fig. 5. The profiles are the ones after subtraction of background. The crystalline reflections for the P(3HB) and the 3HB-rich copolymers could be indexed on the basis of P(3HB) α -form structure (Yokouchi et al., 1973) while the crystalline phase of P(3HB-co-97mol%-4HB) fibers adopted the P(4HB) crystal structure (Su et al., 2003).

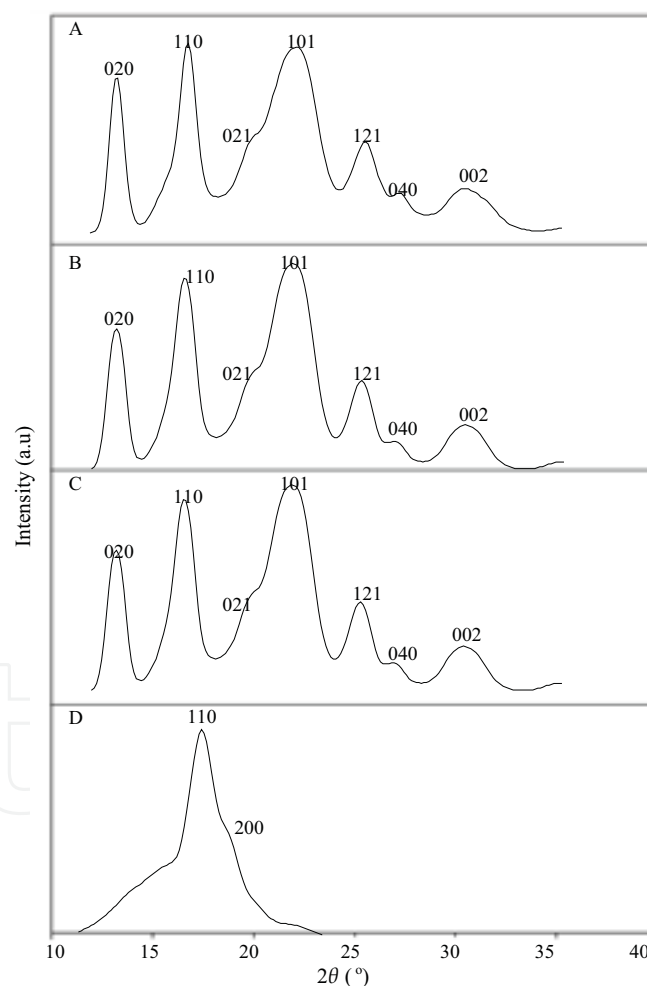


Fig. 5. Integrated 1D profiles from 2D WAXD patterns of as-spun: A. P(3HB) , B. P(3HB-co-5mol%-3HHx), C. P(3HB-co-7mol%-4HB) and D. P(3HB-co-97mol%-4HB).

The WAXD profiles of the as-spun PLLA and stereocomplexed PLA are shown in Fig. 6. The PLLA nanofibers show diffraction peaks at $2\theta = 15.1^\circ$, 16.5° (assigned to (100)/ (200)), and 18.1° that are assigned to the α -form homocrystal of PLLA. The stereocomplexed PLA

nanofibers showed diffraction peaks at $2\theta = 12.0^\circ$ (assigned to (100)), 20.8° and 24.1° that are assigned only to the stereocomplex crystal of PLA (Hasirci et al., 2001). This result confirms that the stereocomplexed PLA nanofibers solely consist of the stereocomplex crystal and not the homocrystal of PLLA and PDLA (Ishii et al., 2007).

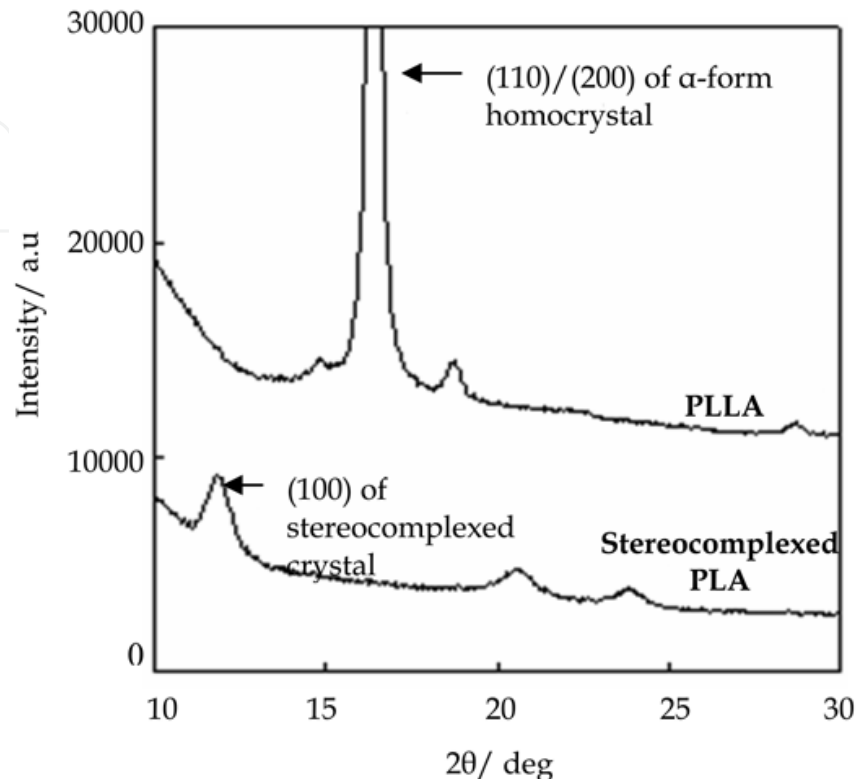


Fig. 6. Wide-angle X-ray diffraction patterns of the electrospun PLLA and stereocomplexed PLA.

From the 1D profiles, the crystallinities of as-spun, sterilized and nanofibrous scaffolds after *in vivo* and *in vitro* studies are estimated, according to the method described above. As shown in Figs. 7 and 8, the crystallinities of the as-spun scaffolds increased in the order of $P(3HB-co-97mol\%-4HB) \ll P(3HB-co-5mol\%-3HHx) \approx P(3HB-co-7mol\%-4HB) < \text{Stereocomplexed PLA} < P(3HB) < PLLA$. The bulk material equivalents of PHA show the same tendency in crystallinity content (Doi et al., 1992). It has been reported that the crystallinity of P(4HB) homopolymer is much lower than that of P(3HB) homopolymer (Saito et al., 1996). The slight lowering of the crystallinities of the 3HB-rich copolymers is due to the exclusion of second monomer unit from the crystalline lattice (Di Lorenzo et al., 2001). It is evident that the degradability of the nanofibrous scaffolds, as shown in Figs. 2 and 3, strongly depends on the crystallinity.

It was confirmed that the EtO sterilization did not appear to have any effect on the crystallinities of all the PHA and PLA-based nanofibrous scaffolds. It was described earlier that partial melting might occur during the sterilization of P(3HB-co-97mol%-4HB). Even if so, the crystallinity will surely recover after the sterilization. The crystallinities of the PHA nanofibrous scaffolds after the *in vivo* and *in vitro* studies remained unchanged. But, it should be noted that the scaffolds for X-ray measurements are the retrieved or remained ones after *in vivo* and *in vitro* experiments. The crystallinity of the P(3HB-co-97mol%-4HB), which shows obvious bioabsorption or degradation in SEM observation, also little changed

even after implantation in rat. This means that the degradation of nanofibrous scaffolds progresses preferentially from the surface of the nanofibrous scaffolds or interface which contacts with the tissues of rat. It is deduced that some substance such as tissue enzymes facilitate the degradation (Gogolewski, 1992).

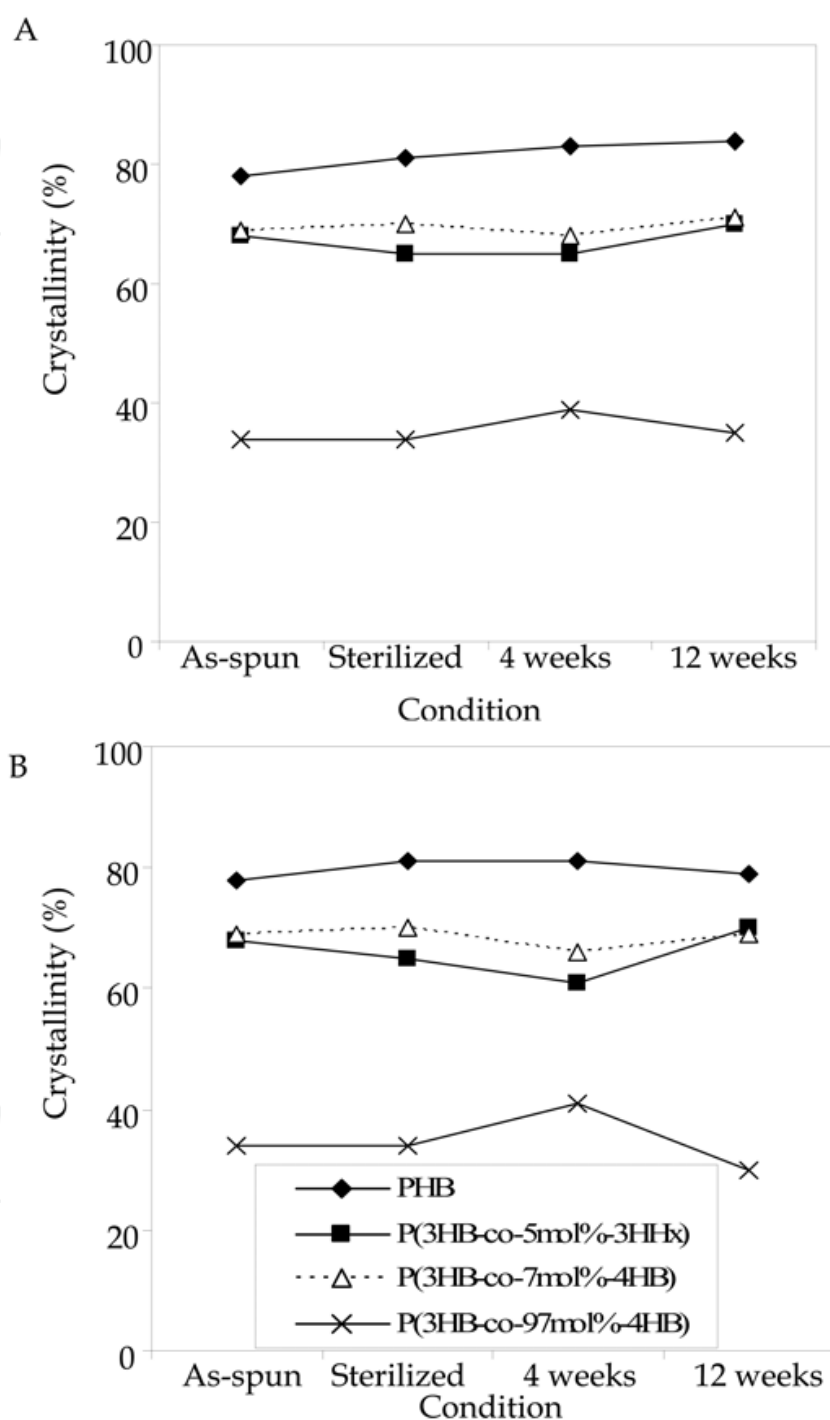


Fig. 7. Crystallinities of the electrospun PHA in different conditions: A. *in vivo* and B. *in vitro*.

After 4 weeks of implantation, the PLLA nanofibrous scaffold showed 28% decrease in crystallinity (86% to 58%) while the electrospun stereocomplexed PLA scaffold showed 12%

decrease in crystallinity (61% to 49%) (Fig. 8). These results support the higher stability of the stereocomplexed PLA nanofibrous scaffold than the PLLA nanofibrous scaffold, as seen from the visual inspection of the explanted nanofibrous scaffolds.

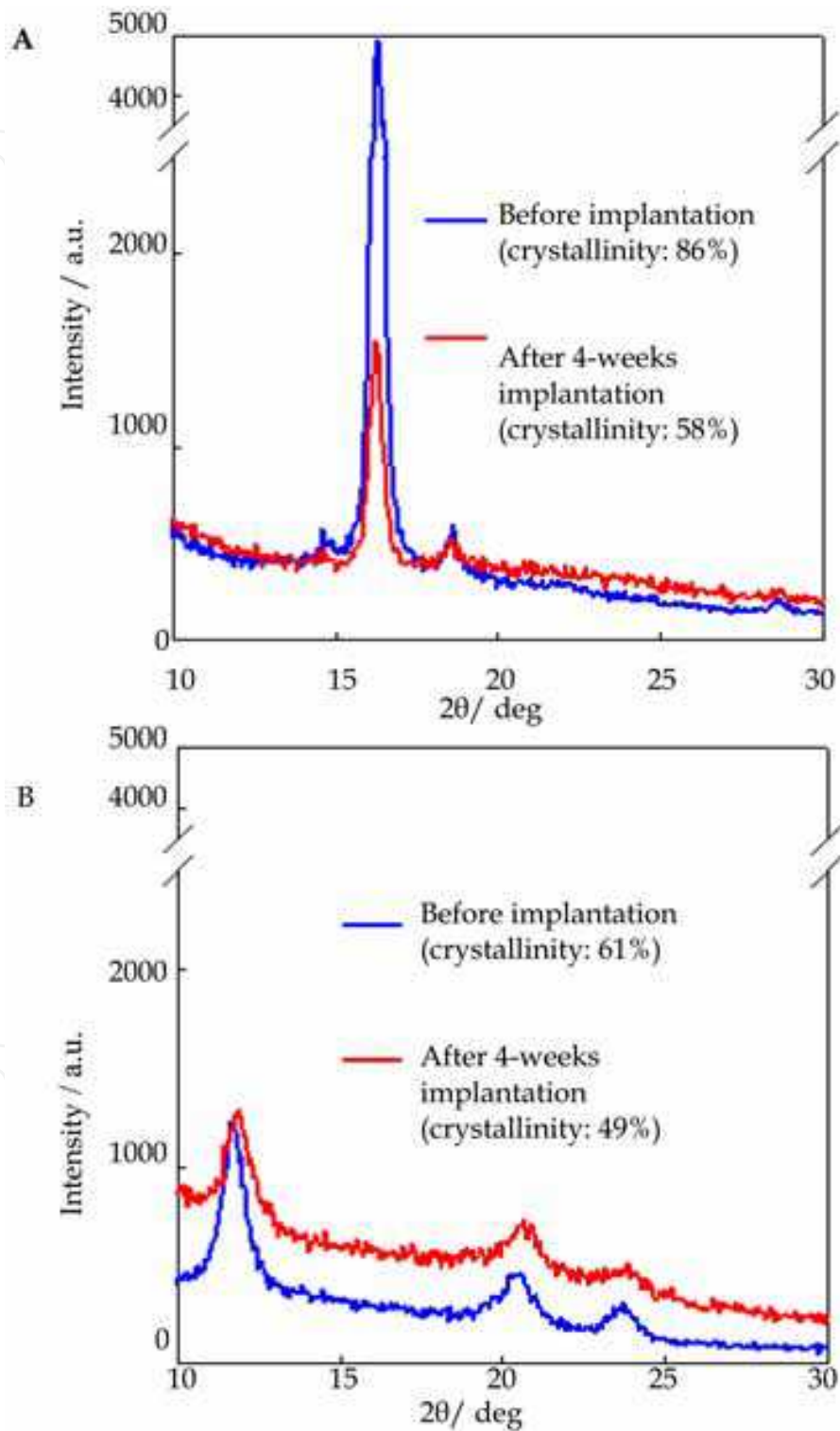


Fig. 8. WAXD patterns of A. PLLA and B. stereocomplexed PLA nanofibrous scaffolds before and after 4 weeks of implantation.

3.3 Molecular weight changes of nanofibrous scaffolds

GPC analysis was carried out to investigate the possible occurrence of molecular chain cleavage (as suggested by SEM and WAXD observations) *in vivo*. Table 1 summarizes the change in M_w and polydispersity index (M_w / M_n) for the as-spun scaffolds and scaffolds following sterilization, 4 and 12 weeks of *in vivo* and *in vitro* studies.

| Material | Condition | $M_w \times 10^5$ | M_w / M_n | |
|----------------------|-------------------------|-------------------|-----------------|-----------------|
| P(3HB) | As-spun | 11 | 3.1 | |
| | Sterilized | 9.1 | 3.3 | |
| | 4 weeks <i>in vivo</i> | <i>in vivo</i> | 12 | 2.6 |
| | | <i>in vitro</i> | 11 | 2.6 |
| | 12 weeks <i>in vivo</i> | <i>in vivo</i> | 8.5 | 2.9 |
| | | <i>in vitro</i> | 17 | 3.3 |
| P(3HB-co-5mol%-3HHx) | As-spun | 13 | 3.6 | |
| | Sterilized | 12 | 3.6 | |
| | 4 weeks <i>in vivo</i> | <i>in vivo</i> | 12 | 3.1 |
| | | <i>in vitro</i> | 11 | 4.3 |
| | 12 weeks <i>in vivo</i> | <i>in vivo</i> | 11 | 3.3 |
| | | <i>in vitro</i> | 13 | 4.3 |
| P(3HB-co-7mol%-4HB) | As-spun | 7.0 | 3.0 | |
| | Sterilized | 6.8 | 3.0 | |
| | 4 weeks <i>in vivo</i> | <i>in vivo</i> | 6.4 | 2.6 |
| | | <i>in vitro</i> | 6.1 | 2.6 |
| | 12 weeks <i>in vivo</i> | <i>in vivo</i> | 3.9 | 2.7 |
| | | <i>in vitro</i> | 5.0 | 2.6 |
| P(3HB-co-97mol%-4HB) | As-spun | 1.7 | 1.5 | |
| | Sterilized | 1.9 | 1.8 | |
| | 4 weeks <i>in vivo</i> | <i>in vivo</i> | 1.0 | 1.6 |
| | | <i>in vitro</i> | 2.5 | 2.0 |
| | 12 weeks <i>in vivo</i> | <i>in vivo</i> | 1.2 | 2.0 |
| | | <i>in vitro</i> | 2.2 | 1.8 |
| PLLA | As-spun | 8.7 | 2.3 | |
| | Sterilized | 8.7 | 2.3 | |
| | 4 weeks <i>in vivo</i> | <i>in vivo</i> | 7.2 | 2.4 |
| | | <i>in vitro</i> | 4.9 | 3.5 |
| | 12 weeks <i>in vivo</i> | <i>in vivo</i> | 3.9 | 2.3 |
| | | <i>in vitro</i> | 5.4 | 3.0 |
| Stereocomplexed PLA | As-spun | 2.8 | 3.3 | |
| | Sterilized | 2.9 | 3.3 | |
| | 4 weeks <i>in vivo</i> | <i>in vivo</i> | 2.6 | 2.3 |
| | | <i>in vitro</i> | 2.5 | 3.0 |
| | 12 weeks <i>in vivo</i> | <i>in vivo</i> | ND ^a | ND ^a |
| | | <i>in vitro</i> | 2.5 | 2.2 |

Table 1. Molecular weight properties of the PHA and PLA-based nanofibrous scaffolds.

^aNot determined due to poor solubility in chloroform.

After sterilization, all of the nanofibrous scaffolds showed no significant differences in their molecular weight. Despite the large surface area of the fibers, the PHA nanofibrous scaffolds remained intact in the *in vitro* study because they have higher resistance to hydrolysis in non-biological environment where specific enzymes are absent (Doi et al, 1992; Marois et al., 2000). Furthermore, the immersion in PBS (pH 7.4) under sterile conditions up to only 12 weeks is short and the temperature is too low for any significant hydrolysis to occur. The subcutaneous implantation, however, seems to cause decrease in the M_w of PHA copolymers with 4HB unit. At 4 weeks, bioabsorption was the most pronounced for the P(3HB-co-97mol%-4HB) nanofibrous scaffold with 47% loss M_w , while the M_w of P(3HB-co-7mol%-4HB) showed no decrease. Following longer implantation period, the P(3HB-co-7mol%-4HB) lost 43% of M_w . Unexpectedly, the P(3HB-co-97mol%-4HB) recorded only 37% of M_w loss after 12 weeks. A possible reason for this observation is that the remaining P(3HB-co-97mol%-4HB) nanofibrous scaffold that was retrieved could consist of only higher molecular weight fraction as the biodegraded products of lower molecular weight diffused away more easily. The GPC data confirmed that the number of main-chain carbon atom strongly influences the rate of hydrolysis for the PHA nanofibrous scaffolds.

In the case of the PLA-based nanofibrous scaffolds, bioabsorption was obvious after 4 weeks implantation in rat. The PLLA nanofibers recorded a higher bioabsorption rate (17%) than the stereocomplexed PLA nanofibers (10%) and continued to decrease until 12 weeks of implantation in rat. The GPC data of the stereocomplexed PLA nanofibrous scaffold after 12 weeks implantation were not obtained due to its poor solubility in chloroform. After 4 weeks of exposure to PBS, the stereocomplexed PLA nanofibrous scaffold only lost 14% of its M_w but the PLLA nanofibrous scaffold lost 44% of its M_w . However, the degradation rate of the PLLA nanofibrous scaffold slowed down after 12 weeks in PBS while the stereocomplexed PLA nanofibrous scaffold continued to show increase of up to 31% M_w loss. The GPC data of the *in vitro* experiment suggest that the stereocomplexed PLA nanofibrous scaffold has higher resistance to hydrolysis compared to the PLLA nanofibrous scaffold and are in accordance to the SEM observations. Literature have reported that the strong interaction (even when they are in an amorphous state) between the PLLA chains and the PDLA chains in the stereocomplexed PLA has made it more hydrolysis-resistant than non-blended PLLA and PDLA specimens (Tsuji, 2005). Tsuji et al., confirmed the above by preparing various types of equimolarly blended specimens from PLLA and PDLA and performed their hydrolytic degradation in PBS (pH 7.4) at 37°C together with non-blended PLLA and PDLA specimens (Tsuji, 2002; Tsuji et al., 2003). They observed retarded hydrolytic degradation of the blended specimens compared with the non-blended specimens, irrespective of their state, amorphous or homo-crystallized.

Overall, the rate of bioabsorption of the PLA-based nanofibrous scaffolds was confirmed to be slower than those of the 4HB-rich scaffold but faster than the 3HB-rich nanofibrous scaffolds. Thus, the GPC data are in good agreement with the results obtained in SEM and WAXD analyses.

3.4 Mechanical properties of nanofibrous scaffolds

Table 2 summarizes the mechanical properties of the obtained PHA and PLA-based nanofibrous scaffolds.

| Material | Condition | Mechanical properties | |
|-----------------------|-------------------------|------------------------|-----------------------|
| | | Tensile strength (MPa) | Young's Modulus (MPa) |
| P(3HB) | As-spun | 17 | 223 |
| | Sterilized | 15 | 234 |
| | 4 weeks <i>in vivo</i> | 12 | 182 |
| | <i>in vitro</i> | 14 | 220 |
| | 12 weeks <i>in vivo</i> | 15 | 152 |
| | <i>in vitro</i> | 13 | 194 |
| P(3HB-co-5mol%- 3HHx) | As-spun | 15 | 277 |
| | Sterilized | 12 | 272 |
| | 4 weeks <i>in vivo</i> | 12 | 268 |
| | <i>in vitro</i> | 13 | 208 |
| | 12 weeks <i>in vivo</i> | ND ^b | ND ^b |
| | <i>in vitro</i> | 15 | 230 |
| P(3HB-co-7mol%-4HB) | As-spun | 8 | 184 |
| | Sterilized | 8 | 139 |
| | 4 weeks <i>in vivo</i> | ND ^b | ND ^b |
| | <i>in vitro</i> | 8 | 163 |
| | 12 weeks <i>in vivo</i> | ND ^b | ND ^b |
| | <i>in vitro</i> | 9 | 110 |
| P(3HB-co-97mol%- 4HB) | As-spun | 13 | 9 |
| | Sterilized | 15 | 16 |
| | 4 weeks <i>in vivo</i> | 4 | 12 |
| | <i>in vitro</i> | 11 | 14 |
| | 12 weeks <i>in vivo</i> | ND ^b | ND ^b |
| | <i>in vitro</i> | 14 | 16 |
| PLLA | As-spun | 6 | 143 |
| | Sterilized | 6 | 143 |
| | 4 weeks <i>in vivo</i> | ND ^b | ND ^b |
| | <i>in vitro</i> | 11 | 130 |
| | 12 weeks <i>in vivo</i> | ND ^b | ND ^b |
| | <i>in vitro</i> | 12 | 123 |
| Stereocomplexed PLA | As-spun | 6 | 94 |
| | Sterilized | 6 | 94 |
| | 4 weeks <i>in vivo</i> | 9 | 80 |
| | <i>in vitro</i> | 13 | 78 |
| | 12 weeks <i>in vivo</i> | ND ^b | ND ^b |
| | <i>in vitro</i> | 12 | 83 |
| Skin ^a | | 5-30 | 15-150 |

Table 2. Mechanical properties of the nanofibrous scaffolds.

^aData obtained from Zong et al., 2005.

^bNot determined as the retrieved scaffolds from rat had cracks on the surface that prevented tensile test.

The mechanical properties of all the as-spun scaffolds were comparable to those of human skin, and hence suggest they are mechanically stable in supporting regenerated tissues. The

Young's modulus of the as-spun nanofibrous scaffolds increased in the order of P(3HB-co-97mol%-4HB) \ll Stereocomplexed PLA $<$ P(3HB-co-7mol%-4HB) $<$ PLLA $<$ P(3HB) $<$ P(3HB-co-5mol%-3HHx). Low Young's modulus, that is, high elasticity is a characteristic property in rubber-state amorphous polymers. Accordingly, this indicates that the P(3HB-co-97mol%-4HB) fibers are more amorphous than the other nanofibrous scaffolds, and this is consistent with the WAXD results. The distinct mechanical properties of the nanofibrous scaffolds could find different use in tissue engineering. For example, the 3H-Brich and PLA-based nanofibrous scaffolds which are more rigid could serve as preferential substrates for directional cell migration (Lo et al., 2000) while the compliant 4HB-rich nanofibrous scaffold could be used to promote cell motility (Pelham et al., 1997) or for soft-tissue engineering. The EtO sterilization and the immersion in PBS buffer little affected the mechanical properties of all PHA nanofibrous scaffolds. Interestingly, the bioabsorption in rat and degradation in PBS resulted in greater plasticization of the PLA-based nanofibrous scaffolds than those of the PHA nanofibrous scaffolds, as evidenced by the increase in their tensile strength.

4. Tissue response and mechanism of bioabsorption of PHA and PLA-based nanofibrous scaffolds

4.1 Tissue response of nanofibrous scaffolds

Histological observations give important information about the degree of inflammatory reactions and the penetration of the surrounding tissues into the implanted scaffolds. The histological sections of the nanofibrous scaffolds at different period of subcutaneous implantation are shown in Figs. 9 and 10. The nuclei of the inflammatory cells or macrophages were stained blue by the hematoxylin dye and their presence is an indication of tissue response towards the implanted scaffolds.

Histological observations indicate that all the three PHA copolymers nanofibrous scaffolds elicited fairly mild tissue response relative to that of the P(3HB) nanofibrous scaffold throughout the course of study. After 4 weeks of implantation, some parts of the P(3HB-co-97mol%-4HB) nanofibrous scaffold bordering the interface were degraded as evidenced by the small fragments broken off from the main scaffold (Fig. 9 D4). More macrophages were found to be present along the interface connected to this copolymer in comparison to the P(3HB-co-7mol%-4HB) and P(3HB-co-5mol%-3HHx) nanofibrous scaffolds (Figs. 9 C4 and 9 D4). This phenomenon is desirable during wound healing because the presence of macrophages is necessary for the regeneration of many cell types (Rappolee et al., 1988). Macrophages clear the way for tissue ingrowths by phagocytosis of damaged tissue, necrotic and apoptotic cells and environment particles. They also secrete a spectrum of cytokines and growth factors to regulate cell recruitment, proliferation and differentiation which lead to effective tissue regeneration and angiogenesis. In fact, studies of wound healing have shown that if macrophage infiltration is prevented, then healing is severely impaired (Martin, 1997; Leiboyich et al., 1975).

The presence of thin connective tissue surrounding the P(3HB-co-97mol%-4HB) nanofibrous scaffold was also observed. The most promising finding was the tissue response after 12 weeks of implantation for the P(3HB-co-97mol%-4HB) nanofibrous scaffold. No fibrous encapsulation was observed around the degraded copolymer and there was also a substantial drop in the number of inflammatory cells (Fig. 9 B12). This observation is similar to a study done on the biocompatibility of P(4HB) implanted subcutaneously in rats by Martin and co-workers (Martin et al., 1999) that reported minimal inflammatory responses.

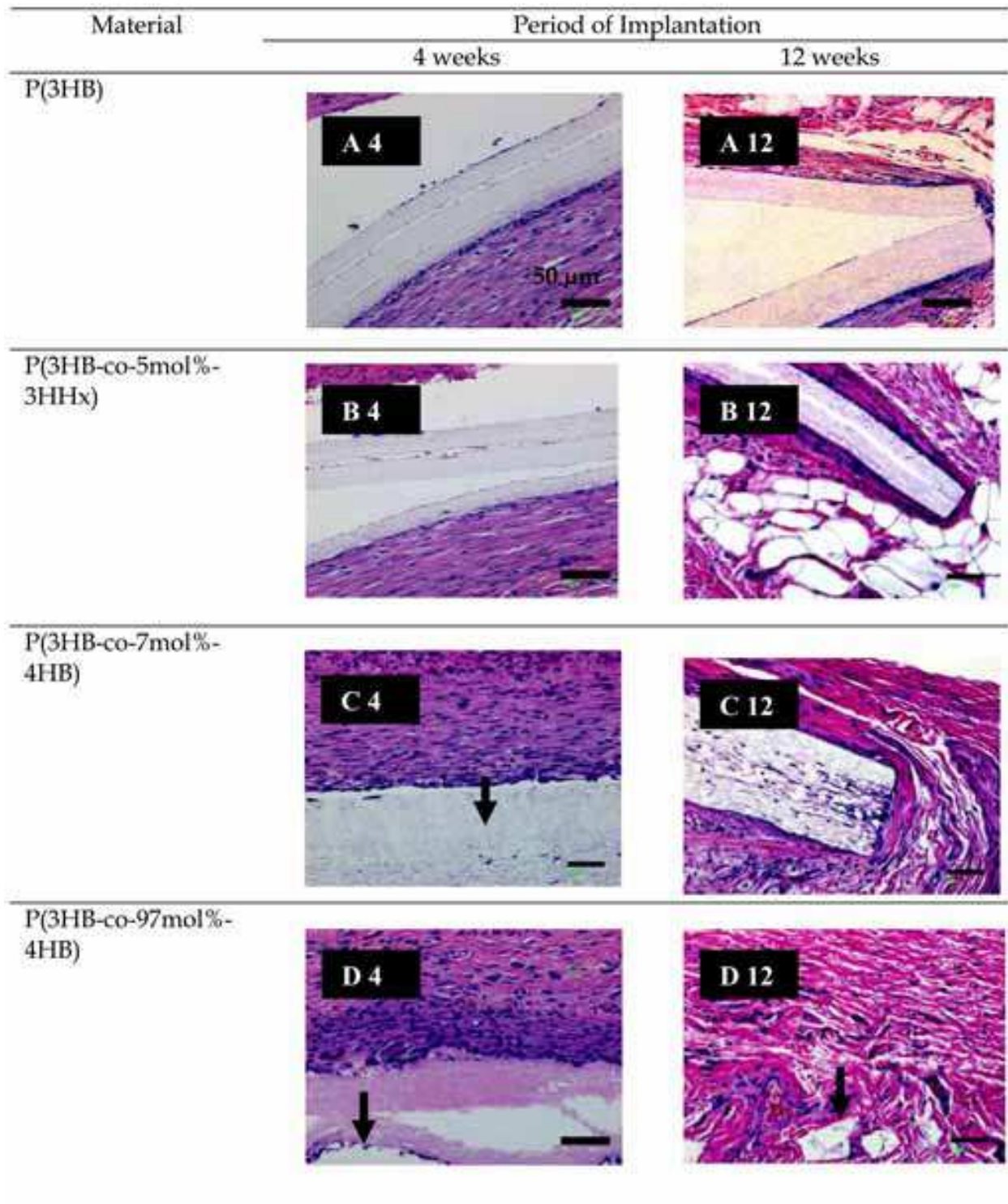


Fig. 9. Histological sections of the PHA nanofibrous scaffolds at different period of subcutaneous implantation. Arrows indicate the polymer surface.

In this study, the number of inflammatory cells surrounding the P(3HB-co-7mol%-4HB) and P(3HB-co-5mol%-3HHx) nanofibrous scaffolds did not appear to have lessened. The muscle cells surrounding these two scaffolds appeared compact as a result of inflammatory reaction (Figs. 9B and 9C). After 12 weeks of implantation, the number of macrophages bordering the

P(3HB) increased. Inflammation was obvious due to the compacted muscle cells surrounding the scaffold. The difference in tissue response to the P(3HB-co-97mol%-4HB) and the nanofibrous scaffolds with higher molar fraction of 3HB reflected their distinct physical properties. It has been reported that rigid polymer, such as P(3HB), elicit acute inflammatory reaction because it exerts a continuous mechanical stimulus to the surrounding tissues of the implants (Qu et al., 2006). Although the tissue response to the P(3HB-co-7mol%-4HB) and electrospun P(3HB-co-5mol%-3HHx) nanofibrous scaffolds was slightly more pronounced than that of the P(3HB-co-97mol%-4HB), the overall local tissue response to all three copolymers were found to be mild. The results have confirmed the biocompatibility of all three types of PHA copolymers.

For the PLA-based nanofibrous scaffolds, their presence *in vivo* brought stronger tissue response in comparison to the PHA nanofibrous scaffolds. As indicated in Fig. 10 A4, a thick layer of inflammatory cells was accumulated at the interface between the PLLA nanofibrous scaffold and the surrounding tissues. In contrast, the layer of accumulated inflammatory cells was thinner for the stereocomplexed PLA nanofibrous scaffold (Fig. 10 B4). This indicates that the stereocomplexed PLA nanofibrous scaffold induces smaller degree of tissue response than the PLLA nanofibrous scaffold. Interestingly, delamination (indicated by the ellipsoid in Fig. 10 A4) occurred on the surface of the PLLA nanofibrous scaffold and hence the infiltration of the surrounding tissues was observed. After 12 weeks of implantation, the PLLA nanofibrous scaffold was significantly fragmented as indicated by

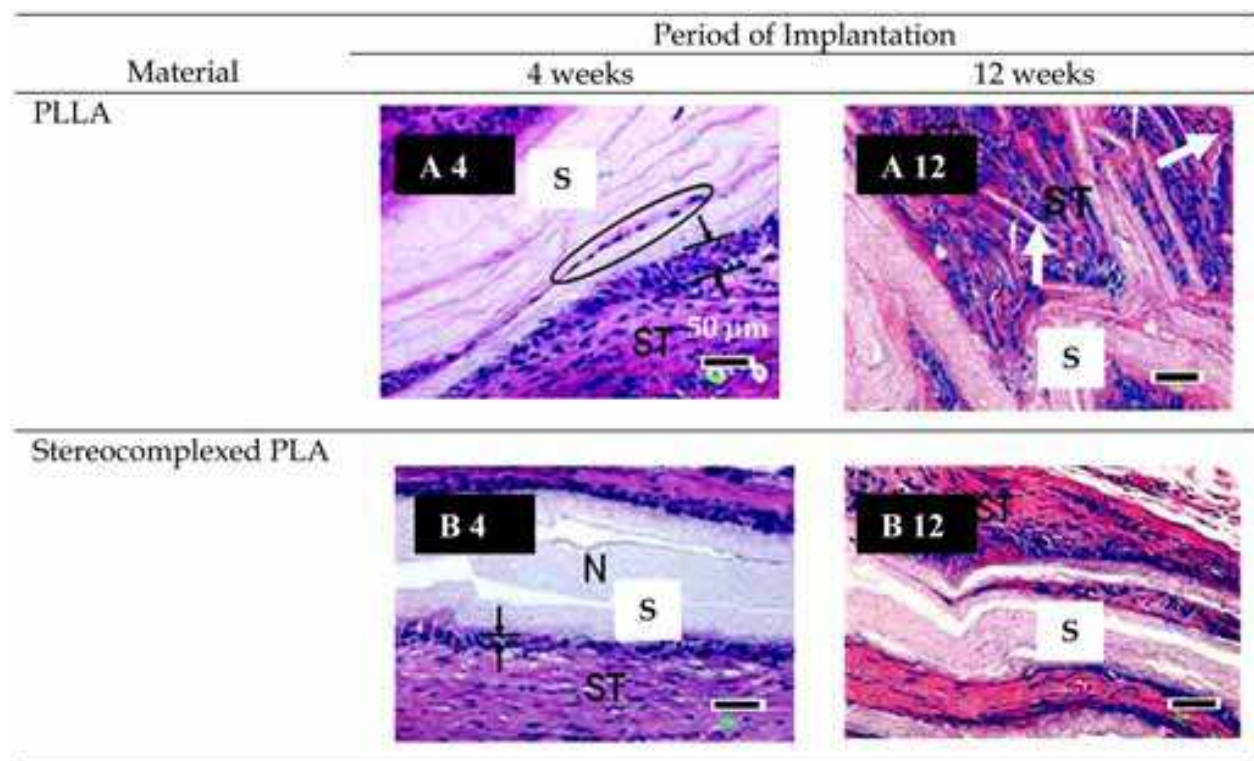


Fig. 10. Histological sections of the PLA-based nanofibrous scaffolds at different period of subcutaneous implantation. The width of inflammatory cells is indicated by the arrows and lines in A4 and B4. Ellipsoid region in A4 and white arrows in A12 indicate the infiltration of surrounding tissues and fragmented fibers, respectively. ST: surrounding tissues; S: scaffold.

the white arrows in Fig. 10 A12, but the stereocomplexed PLA nanofibrous scaffold retained its original morphology. These trends are well correlated with the bulk appearances of the scaffolds and further confirm that the bioabsorption of the stereocomplexed PLA nanofibrous scaffold proceeds slower than that of the PLLA nanofibrous scaffold.

From the histological observations, the biocompatibility of the P(3HB-co-97mol%-4HB) nanofibrous scaffold is by far the most superior among all of the electrospun scaffolds investigated in this current work. In addition, the *in vitro* toxicity of the P(3HB-co-4HB) biosynthesized from *D. acidovorans* which was determined by Siew and co-workers also demonstrated that this copolymer has good biocompatibility (Siew et al., 2007). Their recent genotoxicity study also revealed encouraging results for this PHA copolymer (Siew et al., 2008). The acidic products from the degradation of PLA-based scaffolds act to catalyze further degradation which brings on accumulation of acidic products at the implant site and elicit stronger inflammatory response. Hence, it is not surprising that all PHA nanofibrous scaffolds outperformed the PLA-based nanofibrous scaffolds in terms of tissue response.

4.2 Mechanism of bioabsorption of nanofibrous scaffolds

4.2 (a) PHA nanofibrous scaffolds

The results from various analyses clearly demonstrated that the bioabsorption rate of the P(3HB-co-97mol%-4HB) was the fastest relative to the other two PHA copolymers. Three possible reasons for this observation are as follows: Firstly, the P(3HB-co-97mol%-4HB) with low crystallinity is more susceptible to bioabsorption as water and enzymes penetrate easier into the amorphous regions. Secondly, previous studies have established that macrophages are able to phagocytize PHA *in vitro* (Ali et al., 1994; Saad et al., 1999) and free radicals, acidic products or enzymes produced by these cells may also accelerate the degradation (Tracy et al., 1999). The size of the biomaterials determines the way macrophages respond to them (Xia & Triffitt, 2006). Macrophages may phagocytose material particles with sizes smaller than a single-nucleated macrophage (usually around 10 μm in diameter). Large particles between 10 μm and several hundred micrometers in diameter may be engulfed by foreign body giant cells or multinucleated giant cells. For bulk materials in the form of medical devices such as scaffolds, foreign body giant cells will form and adhere to the surface of these materials. As seen in Fig. 9 D4, the number of inflammatory cells was the most concentrated at the interface of electrospun P(3HB-co-97mol%-4HB) suggesting their active part in the bioabsorption process. It is known that biodegradable materials will be degraded within phagosomes after phagocytosis, or eroded via extracellular resorption, with or without the involvement of foreign body giant cells. Also, after total resorption of the biodegradable materials, any associated inflammation will be resolved. Hence, accordingly, the number of macrophages surrounding the P(3HB-co-97mol%-4HB) decreased tremendously after 12 weeks. Thirdly, possibly the enzymatic degradation by lipase also contributed to the rapid bioabsorption of the P(3HB-co-97mol%-4HB). PHA can be enzymatically degraded by PHA depolymerases, but there is no evidence to date that these are present *in vivo* (Williams & Martin, 2002). P(4HB) was found to be also highly susceptible to lipase hydrolysis as opposed to P(3HB) (Mukai et al., 1993). Besides having good mechanical properties and biocompatibility, it is desirable for a medical implant to show good bioabsorption after its primary function has been fulfilled. The persistence of polymer at a wound healing site may lead to chronic inflammation as shown by the slowly degrading P(3HB) patches that elicited a long term (greater than two years)

macrophage response (Malm et al., 1994). Hence the fast bioabsorption rates of the PHA containing 4HB have confirmed their potential in the application for medical implants.

4.2 (b) PLA-based nanofibrous scaffolds

The bioabsorption mechanisms of the PLA-based nanofibrous scaffolds are illustrated in Fig. 11. For the PLLA nanofibrous scaffold, it is believed that intracrystalline swelling induces preferential hydrolysis of the molecular chains in the amorphous regions between lamella crystals. This leads to the cleavage of the fiber strand and the decrease in the molecular weight. Following these events, the chain-end degradation at the edge of the cleaved fiber may occur and leads to the decrease in the crystallinity. The cleavage of the fiber strands may facilitate the delamination and subsequently the fragmentation of the scaffold. The inflammatory reaction at the early stage of implantation may be due to the acidic low-molecular-weight degradation products and the fragmented fibers. A different bioabsorption mechanism is proposed for the stereocomplexed PLA nanofibrous scaffold. It

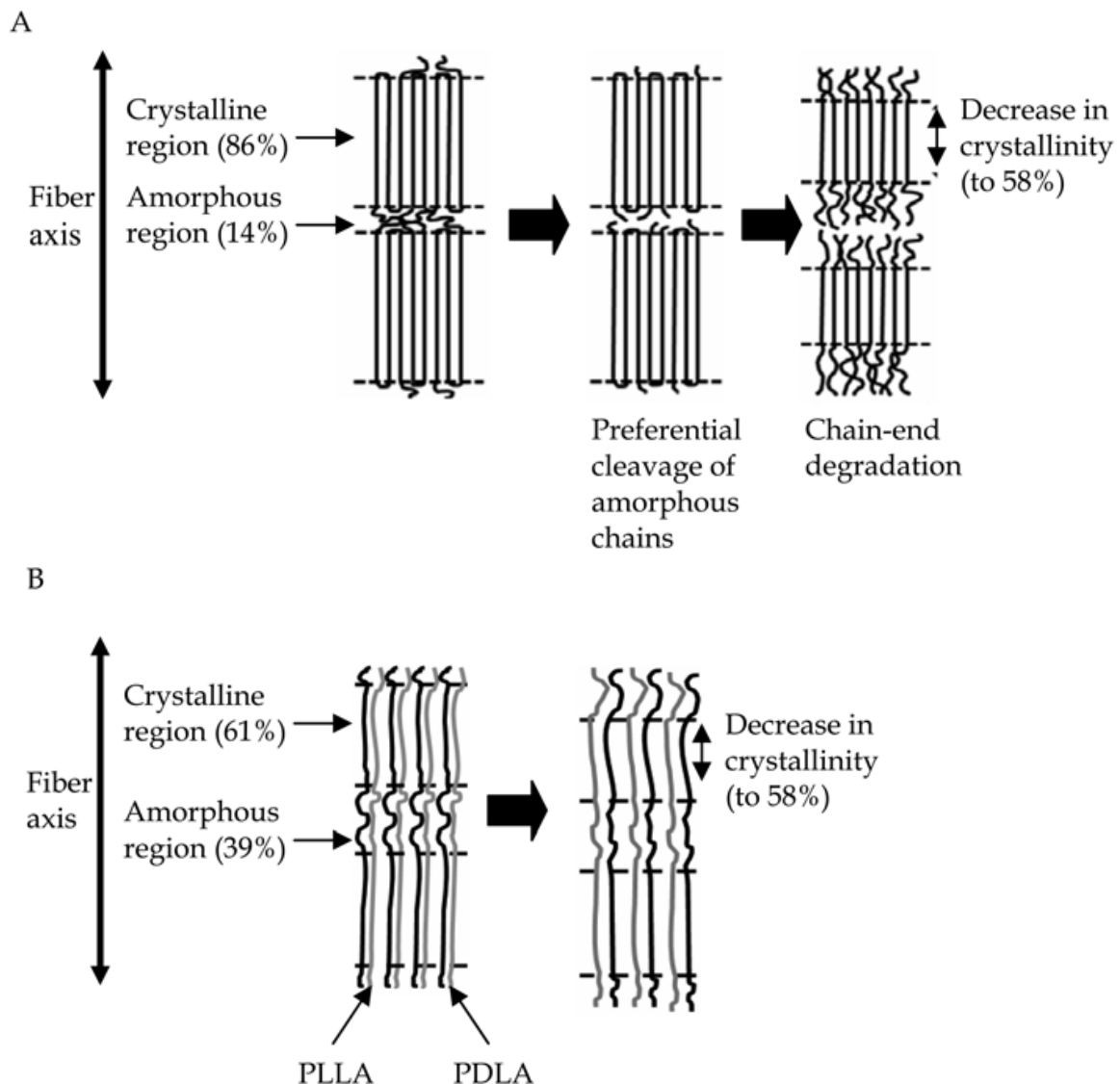


Fig. 11. Schematic representation of the structural changes of A. PLLA and B. stereocomplexed PLA nanofibers during implantation *in vivo*.

is assumed that a single strand of the stereocomplexed PLA nanofiber is composed of the PLLA and PDLA chains aligned in a side-by-side manner. This assumption is made according to the well known fact that the high melting temperature of the stereocomplexed PLA is caused by the strong molecular interaction between the PLLA and PDLA chains. This particular molecular arrangement may therefore suppress the hydrolysis of the molecular chains *in vivo*. As such, the morphology of the electrospun stereocomplexed PLA is retained. This also gives the reason why the inflammatory reaction of the stereocomplexed PLA nanofibrous scaffold is limited at the vicinity of the interfacial region between the scaffold and the surrounding tissues.

5. Conclusion

The overall aim of this research was to electrospin P(3HB-co-97mol%-4HB) for fabricating tissue-engineering scaffold with enhanced mechanical properties, bioabsorption and biocompatibility. Its performance as a nanofibrous scaffold for tissue engineering was compared with electrospun homopolymer P(3HB) and its copolymers containing 5mol%-3HHx and 7mol%-4HB as well as with electrospun PLA-based scaffolds. All of these nanofibrous scaffolds were implanted subcutaneously in rats to evaluate their tissue response. Thus far, this is the first study to evaluate the bioabsorption and tissue response of electrospun scaffolds containing 3HB, 3HHx and 4HB monomers implanted in rat models. SEM revealed that both the *in vitro* and *in vivo* surface erosion of the PHA nanofibrous scaffolds progressed dependently on the individual fiber dimensions and monomeric contents. However in the case of the PLA-based nanofibrous scaffolds, SEM showed that despite having similar fiber dimensions, the fragmentation of the PLLA proceeded faster than that of the stereocomplexed PLA. Hence, it is deduced that the molecular chain interactions within the fiber strands strongly influence the fragmentation of PLA-based nanofibers in the *in vitro* and *in vivo* experiments. Sterilization with ethylene oxide did not cause discoloration and damage to all nanofibrous scaffolds. The mechanical properties demonstrated by all nanofibrous scaffolds were comparable to those of human skin, thus suggesting that their structures are able to provide sufficient biomechanical support. For the PHA, nanofibrous scaffolds consisting of high 3HB content had higher degree of crystallinity and thus, they showed slower bioabsorption rate. Even though having rather comparable crystallinity content with the 3HB-rich scaffolds, the bioabsorption rate of PLA-based nanofibrous scaffolds was slightly faster possibly because their smaller fiber dimensions further enhanced hydrolysis. GPC revealed that the *in vitro* degradation of all nanofibrous scaffolds proceeded at a much slower rate in comparison to the bioabsorption *in vivo*. Thus, some enzymes present in the biological environment must have some influence in the bioabsorption of the nanofibrous scaffolds. Histological evaluation showed that subcutaneous implantations of the PHA nanofibrous scaffolds were well tolerated *in vivo* as the tissue response continued to be very mild throughout the course of the study. When compared with the PLA-based nanofibrous scaffolds, the PHA nanofibrous scaffolds showed better biocompatibility because their by-products of degradation did not further induce inflammatory reaction in the body of the rats. The current work also revealed that by changing the molar fraction of monomers in the PHA copolymers, it is possible to create tissue-engineering scaffolds that are tailor-made to meet the various needs in regenerating different cell type. Such versatility would definitely expand the potential of PHAs as biomaterials. Overall, the electrospun P(3HB-co-97mol%-4HB) outperformed all the P(3HB)

copolymers and PLA-based scaffolds in terms of bioabsorbability and biocompatibility, hence proving it to be a promising new biomaterial for tissue engineering scaffold. In conclusion, this research lays the groundwork for a good understanding of the physical properties and tissue response of the electrospun P(3HB-co-97mol%-4HB) nanofibers in their future application as tissue engineering scaffold.

6. Acknowledgement

The authors thank Prof. Won-Ki Lee (Pukyong University, South Korea) and Dr. Toshihisa Tanaka (Shinshu University, Japan) for their kind supply of PDLA and P(3HB-co-7mol%-4HB), respectively. They also thank Dr. Atsushi Mahara (National Cardiovascular Centre, Japan) and Dr. Sunao Murakami (AIST, Japan) for their help in the subcutaneous implantation of nanofiber samples in rats and their retrieval. The authors acknowledge the Asia Program Associate (APA) between Universiti Sains Malaysia and RIKEN Institute. This work was supported by a Grant-in Aid for Scientific Research (B) from the Ministry of Education, Culture Sports, Science and Technology (MEXT) of Japan (No. 19350075) (to T. Iwata) and by a grant for Ecomolecular Science Research II provided by RIKEN Institute.

7. References

- Ali, SAM.; Doherty, PJ. & Williams, DF. (1994). Molecular biointeractions of biomedical polymers with extracellular exudates and inflammatory cells and their effects on the biocompatibility in vivo. *Biomaterials*, Vol. 15, (1994) pp. 779-785
- Anderson, AJ. & Dawes, EA. (1990). Occurrence, metabolic role, and industrial uses of bacterial polyhydroxyalkanoates. *Microbial Review*, Vol. 54, (1990) pp. 450-472
- Demir, MM.; Yilgor, I.; Yilgor, E. & Erman, B. (2002). Electrospinning of polyurethane fibers. *Polymer*, Vol. 43, (2002) pp. 3303-3309
- Di Lorenzo, ML.; Raimo, M.; Cascone, E. & Martuscelli, E. (2001). Poly(3-hydroxybutyrate)-based copolymers and blends: influence of a second component on crystallization and thermal behavior. *Journal of Macromolecular Science: Physic*, Vol. 40, (2001) pp. 639-667
- Doi, Y.; Kanesawa, Y.; Kawaguchi, Y. & Kunioka, M. (1992). Biodegradation of microbial polyesters in the marine environment. *Polymer Degradability and Stability*, Vol. 32, (1992) pp.173-177
- Dong, H.; Nyame, V.; Macdiarmid, AG. & Jr. Jones, WE. (2004). Polyaniline/Poly(methyl methacrylate) coaxial fibers: The fabrication and effects of the solution properties on the morphology of electrospun core fibers. *Journal of Polymer Science Part B: Polymer Physics*, Vol. 42, (2004) pp. 3934-3942
- FDA clears first of its kind suture made using DNA technology. Available from: FDA News <http://www.fda.gov/bbs/topics/NEWS/2007/NEW01560.html>; 2007 February 12 [accessed 25.04.07]
- Fong, H.; Chun, I. & Reneker, DH. (1999). Beaded nanofibers formed during electrospinning. *Polymer*, Vol. 40, (1999) pp. 4585-4592
- Gogolewski, S. (1992). Resorbable polymers for internal fixation. *Clinical Materials*, Vol. 10, (1992) pp. 13-20
- Griffith, LG. (2000). Emerging design principles on biomaterials and scaffolds for tissue engineering. *Annals of the New York Academy of Sciences*, Vol. 961, (2000) pp. 83-95

- Hasirci, V.; Lewandrowski, K.; Gresser, J.; Wise, DL. & Trantolo DJ. (2001). Versatility of biodegradable biopolymers: degradability and an in vivo application. *Journal of Biotechnology*, Vol. 86, (2001) pp. 135-150
- Ishii, D.; Lee, W.-K.; Kasuya, K. & Iwata, T. (2007). Fine structure and enzymatic degradation of Poly[(R) -3-hydroxybutyrate] and stereocomplexed poly(lactide) nanofibers. *Journal of Biotechnology*, Vol. 132, (2007) pp. 318-324
- Ishii, D.; Tang, HY.; Mahara, A.; Murakami, S.; Yamaoka, T.; Lee, W.-K. & Iwata, T. (2009). *In vivo* tissue response and degradation behavior of PLLA and stereocomplexed PLA nanofibers. *Biomacromolecules*, Vol. 10, (2009) pp. 237-242
- Jeong, EH.; Im, SS. & Youk, JH. (2005). Electrospinning and structural characterization of ultrafine poly(butylene succinate) fibers. *Polymer*, Vol. 4, (2005) pp. 9538-9543
- Leibovich, SJ. & Ross, R. (1975). The role of macrophage in wound repair. A study with hydrocortisone and antimacrophage serum. *American Journal of Pathology*, Vol. 78, (1975) pp. 71-100
- Li, WJ.; Cooper, JA. Jr.; Mauck, RL. & Tuan, RS. (2006). Fabrication and characterization of six electrospun poly(alpha-hydroxy ester)-based fibrous scaffolds for tissue engineering applications. *Acta Biomaterialia*, Vol. 2, (2006) pp. 377-385
- Lo, CM.; Wang, HB.; Dembo, M. & Wang YL. (2000). Cell movement is guided by the rigidity of the substrate. *Biophysical Journal*, Vol. 79, (2000) pp. 144-152
- Lyons, J.; Li, C. & Ko, F. (2004). Melt-electrospinning part I: Processing parameters and geometric properties. *Polymer*, Vol. 45, (2004) pp. 7597-7603
- Malm, T.; Bowald, S.; Bylock, A.; Busch, C. & Saldeen, T. (1994). Enlargement of the right ventricular outflow tract and the pulmonary artery with a new biodegradable patch in transanular position. *European Surgical Research*, Vol. 26, (1994) pp. 298-308
- Marois, Y.; Zhang, Z.; Vert, M.; Deng, X.; Lenz, R. & Guidoin R. (2000). Mechanism and rate of degradation of polyhydroxyoctanoate films in aqueous media: a long term in vitro study. *Journal of Biomedical Material Research*, Vol. 49, (2000) pp. 216-224
- Martin, DP. & Williams, SF. (2003). Medical applications of poly-4-hydroxybutyrate: a strong flexible absorbable biomaterial. *Biochemical Engineering Journal*, Vol. 16 (2003) pp. 97-105
- Martin, DP.; Skraly, FA. & Williams, SF. (1999). Polyhydroxyalkanoate compositions having controlled degradation rates. PCT Patent Application No. WO 99/32536; 1999.
- Martin, P. (1997). Wound healing-aiming for perfect skin regeneration. *Science*, Vol. 276, (1997) pp. 75-81
- Mukai, K.; Doi, Y.; Sema, Y. & Tomita, K. (1993). Substrate specificities in hydrolysis of polyhydroxyalkanoates by microbial esterases. *Biotechnology Letter*, Vol. 15, (1993) pp. 601-604
- Pelham, RJ. & Wang, YL. (1997). Cell locomotion and focal adhesions are regulated by substrate flexibility. *Proceedings of the National Academy of Science*, pp. 13661-13665, Vol. 94, 1997, USA.
- Qu, XH.; Wu, Q.; Zhang, KY. & Chen, GQ. (2006). *In vivo* studies of poly(3-hydroxybutyrate-co-3-hydroxyhexanoate) based polymers: biodegradation and tissue reactions. *Biomaterials*, Vol. 27, (2006) pp. 3540-3548
- Rappolee, DA.; Mark, D.; Banda, MJ. & Werb, Z. (1988). Wound macrophages express TGFalpha and other growth factors in vivo: analysis by mRNA phenotyping. *Science*, Vol. 241, (1988) pp. 708-712

- Saad, B.; Neuenschwander, P.; Uhlschmid, GK. & Suter, UW. (1999) New versatile, elastomeric, degradable polymeric materials for medicine. *International Journal of Biological Macromolecules*, Vol. 25, (1999) pp. 293-301
- Saito, Y.; Nakamura, S.; Hiramitsu, M. & Doi, Y. (1996). Microbial synthesis and properties of poly(3-hydroxybutyrate-co-4-hydroxybutyrate). *Polymer International*, Vol. 39, (1996) pp. 169-174
- Siew, EL.; Rajab, NF.; Osman, A.; Sudesh, K. & Inayat-Hussain, SH. (2007). *In vitro* biocompatibility evaluation of poly(3-hydroxybutyrate-co-4-hydroxybutyrate) copolymer in fibroblast cells. *Journal of Biomedical Research A*, Vol. 81A, (2007) pp. 317-325
- Siew, EL.; Rajab, NF.; Osman, A.; Sudesh, K. & Inayat-Hussain, SH. (2008). Mutagenic and clastogenic characterization of poststerilized poly(3-hydroxybutyrate-co-4-hydroxybutyrate) copolymer biosynthesized by *Delftia acidovorans*. *Journal of Biomedical Materials Research Part A* (in press)
- Su, F.; Iwata, T.; Tanaka, F. & Doi, Y. (2003). Crystal structure and enzymatic degradation of poly(4-hydroxybutyrate). *Macromolecules*, Vol. 36, (2003) pp. 6401-6409
- Subbiah, T.; Bhat, GS.; Tock, RW.; Parameswaran, S. & Ramkumar, SS. (2005). Electrospinning of nanofibers. *Journal of Applied Polymer Science*, Vol. 96, (2005) pp. 557-569
- Tang, HY.; Ishii, D.; Mahara, A.; Murakami, S.; Yamaoka, T.; Sudesh, K.; Samian, R.; Fujita, M.; Maeda, M. & Iwata, T. (2009). Scaffolds from electrospun polyhydroxyalkanoates copolymers: Fabrication, characterization, bioabsorption and tissue response. *Biomaterials*, Vol. 10, (2009) pp. 1307-1317
- Taylor, GI. (1964). Disintegration of water drops in an electric field. *Proceeding of The Royal Society*, pp. 383-397, 1964, London
- Tracy, MA.; Ward, KL.; Firouzabadian, L.; Wang, Y.; Dong, N.; Qian, R. & Zhang, Y. (1999). Factors affecting the degradation rate of poly(lactide-co-glycolide) microspheres *in vivo* and *in vitro*. *Biomaterials*, Vol. 20, (1999) pp. 1057-1062
- Tsuji, H. (2002). Autocatalytic hydrolysis of amorphous-made polylactides: effects of L-lactide content, tacticity, and enantiomeric polymer blending. *Polymer*, Vol. 43, (2002) pp. 1789-1796
- Tsuji, H. (2003). *In vitro* hydrolysis of blends from enantiomeric poly(lactide)s. Part 4: wellhomo-crystallized blends and nonblended films. *Biomaterials*, Vol. 24, (2003) pp. 537-547
- Tsuji, H. (2005). Poly(lactide) Stereocomplexes: Formation, Structure, Properties, Degradation, and Applications. *Macromolecular Bioscience*, Vol. 5, (2005) pp. 567-597
- Williams, SF. & Martin, DP. (2002) Applications of PHAs in medicine and pharmacy. In: Steinbüchel A, editor. Series of biopolymers in 10 volumes, vol. 4. Wiley/VCH/Verlag; 2002. p. 91-121
- Xia, Z. & Triffitt, JT. (2006) A review on macrophages responses to biomaterials. *Biomedical Materials*, Vol. 1, (2006) pp. R1-R9
- Yokouchi, M.; Chatani, Y.; Tadokoro, H.; Teranishi, K. & Tani, H. (1973). Structural studies of polyesters: 5. Molecular and crystal structures of optically active and racemic poly(β -hydroxybutyrate). *Polymer*, Vol. 14, (1973) pp. 267-272

- Zong, X.; Bien, H.; Chung, CY.; Yin, L.; Fang, D.; Hsiao, BS.; Chu, B. & Entcheva, E. (2005). Electrospun fine-textured scaffolds for heart tissue constructs. *Biomaterials*, Vol. 26, (2005) pp. 5330-5338
- Zong, X.; Ran, S.; Kim, KS.; Fang, D.; Hsiao, BS. & Chu, B. (2003). Structure and morphology changes during in vitro degradation of electrospun poly(glycolide-co-lactide) nanofiber membrane. *Biomacromolecules*, Vol. 4, (2003) pp. 416-423
- Zuo, W.; Zhu, M.; Yang, W.; Yu, H.; Chen, Y. & Zhang, Y. (2005). Experimental study on relationship between jet stability and formation of beaded fibers during electrospinning. *Polymer Engineering and Science*, Vol. 45, (2005) pp. 704-709

IntechOpen



Nanofibers

Edited by Ashok Kumar

ISBN 978-953-7619-86-2

Hard cover, 438 pages

Publisher InTech

Published online 01, February, 2010

Published in print edition February, 2010

“There's Plenty of Room at the Bottom” this was the title of the lecture Prof. Richard Feynman delivered at California Institute of Technology on December 29, 1959 at the American Physical Society meeting. He considered the possibility to manipulate matter on an atomic scale. Indeed, the design and controllable synthesis of nanomaterials have attracted much attention because of their distinctive geometries and novel physical and chemical properties. For the last two decades nano-scaled materials in the form of nanofibers, nanoparticles, nanotubes, nanoclays, nanorods, nanodisks, nanoribbons, nanowiskers etc. have been investigated with increased interest due to their enormous advantages, such as large surface area and active surface sites. Among all nanostructures, nanofibers have attracted tremendous interest in nanotechnology and biomedical engineering owing to the ease of controllable production processes, low pore size and superior mechanical properties for a range of applications in diverse areas such as catalysis, sensors, medicine, pharmacy, drug delivery, tissue engineering, filtration, textile, adhesive, aerospace, capacitors, transistors, battery separators, energy storage, fuel cells, information technology, photonic structures and flat panel displays, just to mention a few. Nanofibers are continuous filaments of generally less than about 1000 nm diameters. Nanofibers of a variety of cellulose and non-cellulose based materials can be produced by a variety of techniques such as phase separation, self assembly, drawing, melt fibrillation, template synthesis, electro-spinning, and solution spinning. They reduce the handling problems mostly associated with the nanoparticles. Nanoparticles can agglomerate and form clusters, whereas nanofibers form a mesh that stays intact even after regeneration. The present book is a result of contributions of experts from international scientific community working in different areas and types of nanofibers. The book thoroughly covers latest topics on different varieties of nanofibers. It provides an up-to-date insightful coverage to the synthesis, characterization, functional properties and potential device applications of nanofibers in specialized areas. We hope that this book will prove to be timely and thought provoking and will serve as a valuable reference for researchers working in different areas of nanofibers. Special thanks goes to the authors for their valuable contributions.

How to reference

In order to correctly reference this scholarly work, feel free to copy and paste the following:

Hui Ying Tang, Daisuke Ishii, Kumar Sudesh, Tetsuji Yamaoka and Tadahisa Iwata (2010). Nanofibrous Scaffolds of Bio-Polyesters: In Vitro and In Vivo Characterizations and Tissue Response, Nanofibers, Ashok Kumar (Ed.), ISBN: 978-953-7619-86-2, InTech, Available from:

<http://www.intechopen.com/books/nanofibers/nanofibrous-scaffolds-of-bio-polyesters-in-vitro-and-in-vivo-characterizations-and-tissue-response>

INTECH

open science | open minds

InTech Europe

University Campus STeP Ri
Slavka Krautzeka 83/A
51000 Rijeka, Croatia
Phone: +385 (51) 770 447
Fax: +385 (51) 686 166
www.intechopen.com

InTech China

Unit 405, Office Block, Hotel Equatorial Shanghai
No.65, Yan An Road (West), Shanghai, 200040, China
中国上海市延安西路65号上海国际贵都大饭店办公楼405单元
Phone: +86-21-62489820
Fax: +86-21-62489821

IntechOpen

IntechOpen

© 2010 The Author(s). Licensee IntechOpen. This chapter is distributed under the terms of the [Creative Commons Attribution-NonCommercial-ShareAlike-3.0 License](#), which permits use, distribution and reproduction for non-commercial purposes, provided the original is properly cited and derivative works building on this content are distributed under the same license.

IntechOpen

IntechOpen